

This copy is for your personal, non-commercial use only.

If you wish to distribute this article to others, you can order high-quality copies for your colleagues, clients, or customers by [clicking here](#).

Permission to republish or repurpose articles or portions of articles can be obtained by following the guidelines [here](#).

The following resources related to this article are available online at www.sciencemag.org (this information is current as of July 22, 2010):

Updated information and services, including high-resolution figures, can be found in the online version of this article at:

<http://www.sciencemag.org/cgi/content/full/326/5951/426>

Supporting Online Material can be found at:

<http://www.sciencemag.org/cgi/content/full/326/5951/426/DC1>

This article **cites 21 articles**, 6 of which can be accessed for free:

<http://www.sciencemag.org/cgi/content/full/326/5951/426#otherarticles>

This article has been **cited by** 5 article(s) on the ISI Web of Science.

This article has been **cited by** 3 articles hosted by HighWire Press; see:

<http://www.sciencemag.org/cgi/content/full/326/5951/426#otherarticles>

This article appears in the following **subject collections**:

Development

<http://www.sciencemag.org/cgi/collection/development>

densely packed microbial consortia). Although the loss of nitrate and ammonium from CH₄ seep sediments by catabolic bacterial processes (such as denitrification or anammox) has not yet been determined, these sinks for fixed N may also promote enhanced diazotrophy by the in situ microbial assemblage (3). Additionally, the current discrepancy in the oceanic fixed N budget underscores the possibility of new sources of fixed N in nontraditional and potentially unexpected habitats (1–3, 7). The extent to which the ANME-2/DSS consortia contribute to the putatively missing fraction of global fixed N inputs is unknown, but their input is probably not the only missing term in the equation. N₂ fixation in ANME-2, combined with the diversity of *nifH* genes recovered from marine sediments here and previously (5, 11, 22), suggests that our inventory of marine diazotrophs is incomplete and that we are only beginning to understand the extent and importance of benthic marine N₂ fixation.

References and Notes

- L. A. Codispoti, *Biogeosciences* **4**, 233 (2007).
- C. Mahaffey, A. F. Michaels, D. G. Capone, *Am. J. Sci.* **305**, 546 (2005).
- C. Deutsch, J. L. Sarmiento, D. M. Sigman, N. Gruber, J. P. Dunne, *Nature* **445**, 163 (2007).
- R. W. Fulweiler, S. W. Nixon, B. A. Buckley, S. L. Granger, *Nature* **448**, 180 (2007).
- J. P. Zehr, B. D. Jenkins, S. M. Short, G. F. Stewart, *Environ. Microbiol.* **5**, 539 (2003).
- M. P. Mehta, J. A. Baross, *Science* **314**, 1783 (2006).
- M. C. Horner-Devine, A. C. Martiny, *Science* **320**, 757 (2008).
- D. Karl *et al.*, *Biogeochemistry* **57–58**, 47 (2002).
- W. S. Reebergh, *Chem. Rev.* **107**, 486 (2007).
- M. Strous, M. S. M. Jetten, *Annu. Rev. Microbiol.* **58**, 99 (2004).
- A. Perenthaler *et al.*, *Proc. Natl. Acad. Sci. U.S.A.* **105**, 7052 (2008).
- Information on materials and methods is available on Science Online.
- J. K. Liu, C. H. Liu, C. S. Lin, *Proc. Natl. Sci. Council. Repub. China B* **21**, 37 (1997).
- W. S. Silver, J. R. Postgate, *J. Theor. Biol.* **40**, 1 (1973).
- J. Raymond, *Rev. Mineral. Geochem.* **59**, 211 (2005).
- I. Berman-Frank, P. Lundgren, P. Falkowski, *Res. Microbiol.* **154**, 157 (2003).
- V. J. Orphan, C. H. House, K. U. Hinrichs, K. D. McKeegan, E. F. DeLong, *Science* **293**, 484 (2001).
- C. P. Lechene, Y. Luyten, G. McMahon, D. L. Distel, *Science* **317**, 1563 (2007).
- S. Behrens *et al.*, *Appl. Environ. Microbiol.* **74**, 3143 (2008).
- M. K. Udvardi, D. A. Day, *Annu. Rev. Plant Physiol. Plant Mol. Biol.* **48**, 493 (1997).
- V. J. Orphan, K. A. Turk, A. M. Green, C. H. House, *Environ. Microbiol.* **11**, 1777 (2009).
- H. Dang, X. Luan, J. Zhao, J. Li, *Appl. Environ. Microbiol.* **75**, 2238 (2009).
- J. P. W. Young, in *Genomes and Genomics of Nitrogen-Fixing Organisms*, R. Palacios, W. E. Newton, Eds. (Springer, Netherlands, 2005), pp. 221–241.
- J. A. Leigh, *Curr. Issues Mol. Biol.* **2**, 125 (2000).
- P. A. Murray, S. H. Zinder, *Nature* **312**, 284 (1984).
- S. B. Joye *et al.*, *Chem. Geol.* **205**, 219 (2004).
- J. Brooks *et al.*, *Science* **238**, 1138 (1987).
- D. H. Buckley, V. Huangyuthitham, S. F. Hsu, T. A. Nelson, *Soil Biol. Biochem.* **40**, 1272 (2008).
- P. S. Kessler, C. Daniel, J. A. Leigh, *J. Bacteriol.* **183**, 882 (2001).
- Y.-T. Chien, A. Auerbuch, A. D. Brabban, S. H. Zinder, *J. Bacteriol.* **182**, 3247 (2000).
- We thank C. House, A. Schmitt, K. McKeegan, Y. Guan, J. Eiler, and L. Remusat for assistance with the ion microprobe data collection; S. Joye, M. Boyles, M. Walton, J. Howard, N. Dalleska, O. Mason, A. Green, P. Tavormina, S. Goffredi, C. Gammon, and the shipboard party and crew of the R/V *Atlantis* and DSSV *Alvin* for support in the field and laboratory; and J. Howard, W. Fischer, J. Amend, C. Anderson, D. Fike, D. Sigman, V. Rich, J. Bailey, D. Newman, J. Grotzinger, T. Hoehler, J. Delacruz, and three anonymous reviewers for helpful suggestions regarding this manuscript. Funding was provided by NSF (grant MCB-0348492), the Gordon and Betty Moore Foundation, and an NSF Graduate Research Fellowship (A.E.D.). The Caltech Center for Microanalysis and nanoSIMS 50L are funded by the Gordon and Betty Moore Foundation, and the University of California Los Angeles ion microprobe is partially supported by the NSF Instrumentation and Facilities Program.

Supporting Online Material

www.sciencemag.org/cgi/content/full/326/5951/422/DC1

Materials and Methods

SOM Text

Figs. S1 to S3

Tables S1 to S4

References

25 June 2009; accepted 31 August 2009

10.1126/science.1178223

Generation of Functional Ventricular Heart Muscle from Mouse Ventricular Progenitor Cells

Ibrahim J. Domian,^{1,2*} Murali Chiravuri,^{1*} Peter van der Meer,^{1,3*} Adam W. Feinberg,⁴ Xi Shi,¹ Ying Shao,¹ Sean M. Wu,^{1,2} Kevin Kit Parker,^{2,4,5} Kenneth R. Chien^{1,2,6†}

The mammalian heart is formed from distinct sets of first and second heart field (FHF and SHF, respectively) progenitors. Although multipotent progenitors have previously been shown to give rise to cardiomyocytes, smooth muscle, and endothelial cells, the mechanism governing the generation of large numbers of differentiated progeny remains poorly understood. We have employed a two-colored fluorescent reporter system to isolate FHF and SHF progenitors from developing mouse embryos and embryonic stem cells. Genome-wide profiling of coding and noncoding transcripts revealed distinct molecular signatures of these progenitor populations. We further identify a committed ventricular progenitor cell in the *Isl1* lineage that is capable of limited in vitro expansion, differentiation, and assembly into functional ventricular muscle tissue, representing a combination of tissue engineering and stem cell biology.

The mammalian heart is composed of a diversified set of muscle and nonmuscle cells that arise from multipotent progenitors in the first and second heart field (FHF and SHF, respectively) (1, 2). Defining the precise progenitor identity and the pathways that lead to ventricular myogenesis is critical for understanding cardiogenesis and also for regenerative cardiovascular medicine.

Accordingly, we generated a transgenic mouse with the red fluorescent protein dsRed under the control of an *Isl1*-dependent enhancer of the

Mef2c gene whose expression is restricted to the SHF (3–5). We bred this mouse line with a transgenic mouse line in which enhanced green fluorescent protein (eGFP) is controlled by the cardiac-specific *Nkx2.5* enhancer (6, 7). By fluorescence microscopy of double transgenic embryos on embryonic day 9.5 (E9.5), the entire primitive heart tube was eGFP+, but only the right ventricle (RV) and the outflow tract (OFT) were also dsRed+. Further, the pharyngeal mesoderm (PM), which contributes to the RV and OFT (8, 9), was dsRed+ but eGFP– (Fig. 1, A

to C). To delineate the in vivo expression of the reporters, we performed immunohistochemistry on E9.5 embryos and found that dsRed+/eGFP+ cells (R+G+) were restricted to the RV and OFT, dsRed–/eGFP+ cells (R–G+) to the left ventricle (LV) and inflow tract (IFT), and dsRed+/eGFP– cells (R+G–) to the PM (Fig. 1D).

Embryonic stem cell (ESC) lines make use of many of the in vivo developmental programs, providing an attractive model system for lineage commitment. Therefore, we generated multiple ESC lines that harbor both the *Nkx2.5*-eGFP and the SHF-dsRed reporters (fig. S1A). Fluorescence microscopy of chimeric embryos from these ESC lines revealed faithful recapitulation of marker expression (fig. S1, B and C). In vitro differentiation by embryoid body (EB) formation resulted in discrete populations of R+G+, R+G–, and R–G+ cells by EB day 6 (fig. S1D).

¹Cardiovascular Research Center, Massachusetts General Hospital, Charles River Plaza, CPZN 3200, 185 Cambridge Street, Boston, MA 02114–2790, USA. ²Harvard Stem Cell Institute, Cambridge, MA 02138, USA. ³Department of Cardiology, University Medical Center Groningen, Hanzplein 1, 9700 RB Groningen, Netherlands. ⁴Disease Biophysics Group, School of Engineering and Applied Sciences, Harvard University, Cambridge, MA 02138, USA. ⁵The Wyss Institute for Biologically Inspired Engineering, Harvard University, Boston, MA 02115, USA. ⁶Department of Stem Cell and Regenerative Biology, Harvard University, Cambridge, MA 02138, USA.

*These authors contributed equally to this work.

†To whom correspondence should be addressed. E-mail: krchien@partners.org

To isolate ESC-derived FHF and SHF progenitor cells, we dissociated day 6 EBs into single-cell suspension and fluorescence-activated cell sorting (FACS)-purified four distinct populations

of cells: (i) R+G+, (ii) R+G-, (iii) R-G+, and (iv) unlabeled (R-G-) (Fig. 2A and fig. S2A). We then performed DNA microarray analysis on coding and noncoding RNA. Hierarchical

clustering (10) showed distinct reproducible expression patterns for the different cardiac progenitor subsets of mRNAs, as well as microRNAs (miRNAs) (figs. S3 to S5 and table S1). Next, we

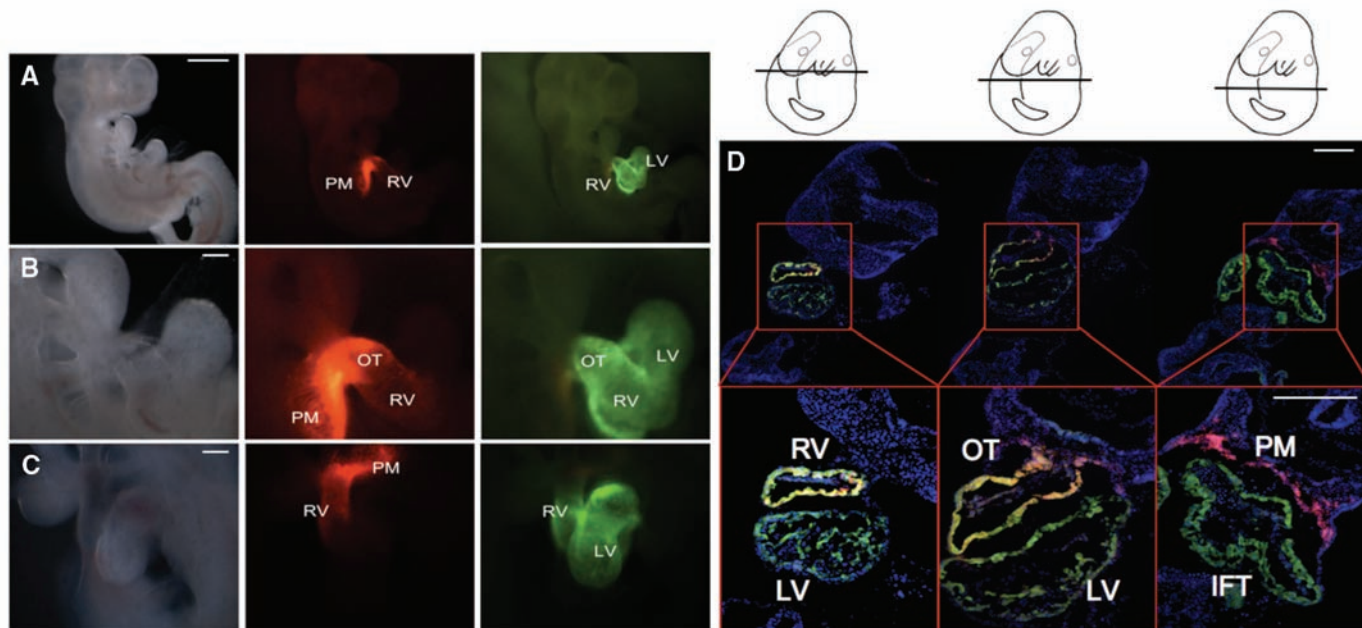


Fig. 1. E9.5 SHF-dsRed/Nkx2.5-eGFP transgenic embryos. (A to C) Whole-mount fluorescence microscopy of double transgenic E9.5 embryos. The LV and IFT are eGFP+ only, the RV and OT are dsRed+ and eGFP+, and the PM is dsRed+. Right lateral [(A) and (B), with (B) as close-up view] and left lateral (C) views are shown. Scale bar, 500 μ m (A);

100 μ m [(B) and (C)]. (D) Immunofluorescence labeling of E9.5 double transgenic mouse embryo shows that cells in the RV and OT are R+G+, in the PM are R+G-, and in the LV and IFT are R-G+. Section levels are shown as a cartoon. eGFP, green; dsRed, red; overlay, yellow. Scale bar, 50 μ m.

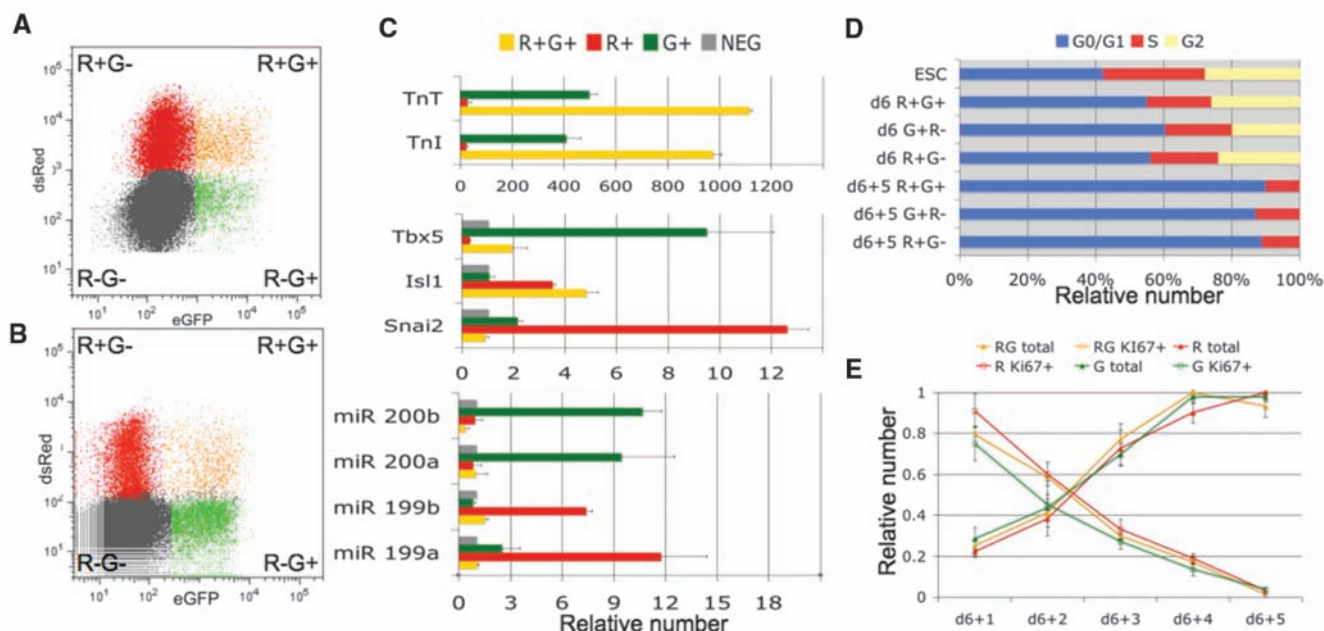


Fig. 2. Isolation of cardiac progenitors. (A and B) Representative flow cytometry plots of double transgenic day 6 EBs (A) and E9.5 embryos (B) showing four populations of cells: (i) R+G+, (ii) R+G-, (iii) R-G+, and (iv) R-G-. (C) QPCR analysis of mRNA and miRNA isolated from embryonic progenitors. Values are normalized against an unlabeled control. Error bars indicate SD. Differences between groups were highly statistically significant

(see tables S2 and S3). (D) Hoechst staining and FACS-based cell cycle analysis of undifferentiated ESCs, EB day6 progenitors, and differentiated progeny. (E) ESC-derived cardiac progenitors were cultured for 5 days. 4',6'-diamidino-2-phenylindole and Ki67 staining was performed to quantify the total cell number and proportion of cycling cells (Ki67+ cells/total cells). Error bars indicate SD ($n = 4$).

FACS-purified E9.5 embryonic progenitors (Fig. 2B and fig. S2B). Quantitative real-time fluorescence polymerase chain reaction (QPCR) analysis on 100 mRNAs and 10 miRNAs revealed that ESC- and embryonic-derived progenitors, isolated immediately after FACS sorting, displayed similar but nonidentical patterns of expression (Fig. 2C and fig. S6). mRNAs and miRNAs implicated in cardiac development and disease were enriched in the colored cells compared with in unlabeled cells. *Isl1*, a marker for the SHF, was appropriately enriched in only the R+G+

and the R+G- populations, whereas T-box transcription factor 5 (*Tbx5*), a marker of the FHF (11, 12), was appropriately enriched only in the R-G+ population. The R+G+ cells appeared to resemble more closely the myogenic population based on the expression of myocardial markers such as cardiac troponins, cardiogenic transcription factors, and bone morphogenetic protein signaling molecules. Further, the R+G- population of the PM expressed high levels of *Snai2*, a transcription factor regulating epithelial-to-mesenchymal transition (EMT) and necessary for cell migration

(13, 14), suggesting that SHF/PM progenitors undergo EMT before migrating during cardiogenesis. In addition, miRNA199a/b were preferentially expressed in the R+G- population, and miRNA200a/b in the R-G+ population, and may therefore be considered cardiac markers for the SHF and FHF, respectively (fig. S7).

Because a hallmark of progenitor cells is their capacity for expansion before differentiation, we performed Hoechst staining and FACS-based cell cycle analysis on undifferentiated ESC, EB day 6

Fig. 3. Differentiation potential of cardiac progenitors. Embryonic- and ESC-derived cardiac progenitors were cultured on fibronectin-coated slides (fibronectin) or micropatterns for 5 days. (A and B) Representative immunofluorescence microscopy of embryonic- (A) or ESC-derived (B) progenitors cultured on micropatterns are shown. Nuclei, blue; smMHC, red; and sarcomeric α -actinin, green. Scale bar, 40 μ m. (C and D) Cell counting was used to quantify the relative number of CM (sarcomeric α -actinin positive) or SM (smMHC positive) derived from embryonic (C) or ESC (D) progenitors. R+G+ populations resulted in the most CM ($P < 0.001$). No significant differences were observed in SM differentiation ($P = 0.38$ to 1.0). P values for the differences in CM differentiation are displayed. Error bars indicate SD ($n = 4$).

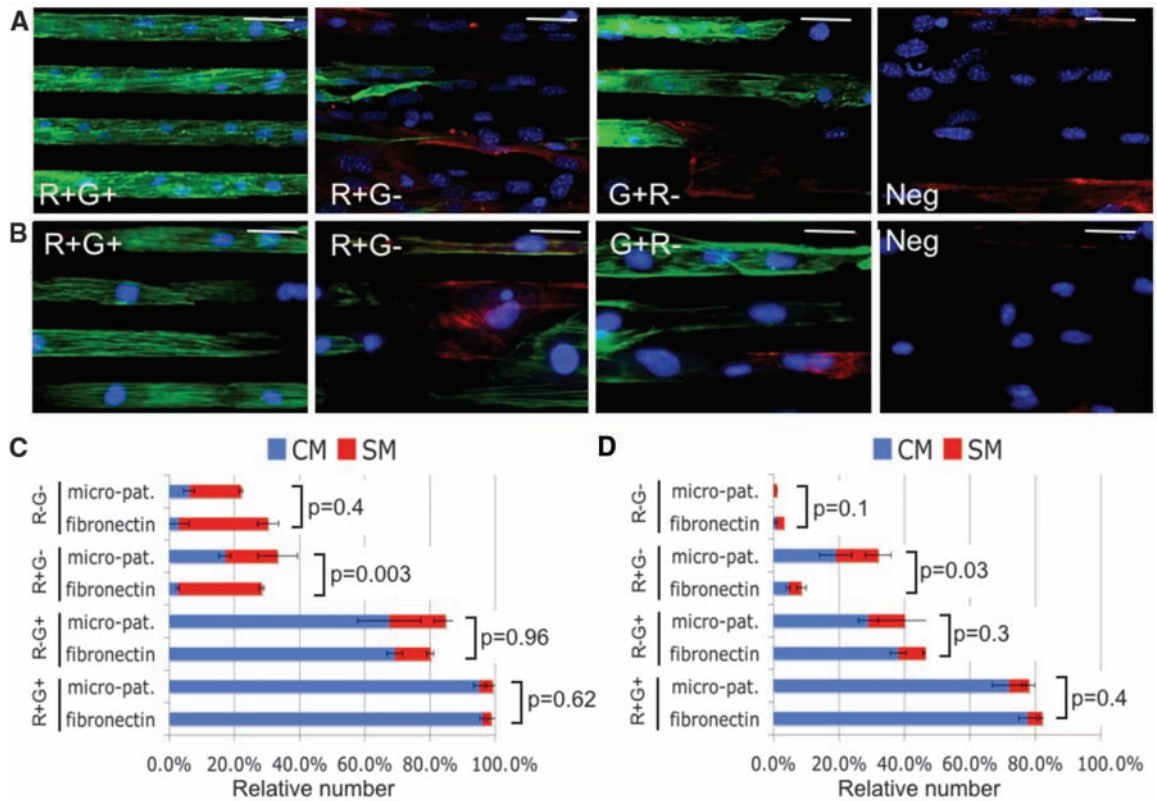
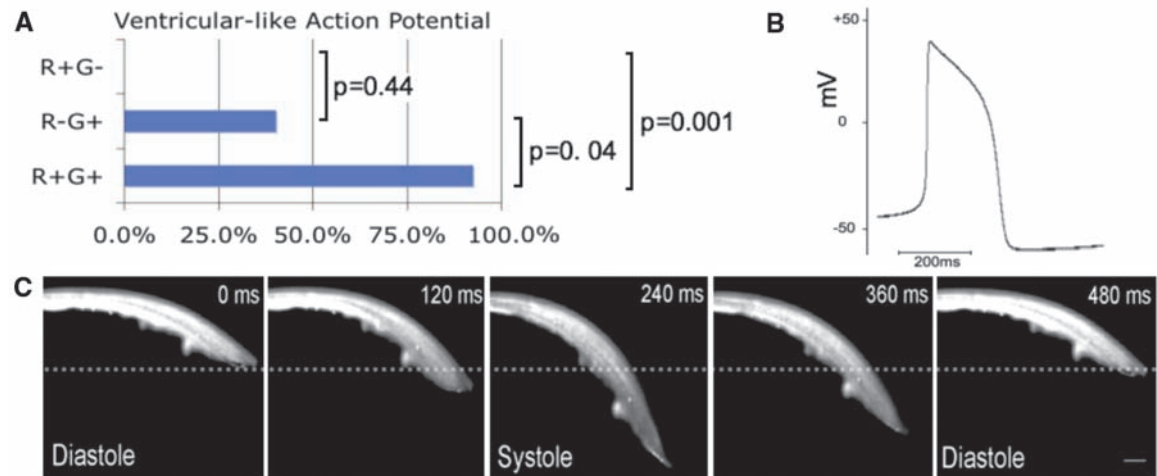


Fig. 4. Engineered ventricular tissue from R+G+ progenitors. (A) R+G+ ($n = 12$), R+G- ($n = 5$), and R-G+ ($n = 5$) progenitors were allowed to differentiate, and single-cell patch clamp recordings were performed. AP morphology was assessed for typical four-phase ventricular AP. (B) Representative spontaneous AP from R+G+ derived cardiomyocytes. (C) ESC-derived R+G+ progenitors were used to generate MTF as described in the SOM and in (15). Field stimulation (10 V, 10-ms pulse width) induced a 0.5-Hz cyclical contraction and rhythmic MTF bending (see movie S1).



cardiac progenitors, and their differentiated progeny (d6+5). ESC and EB day 6 progenitors had 40 to 55% of cells in combined S and G₂ phase, but the differentiated progeny had less than 15% of cells in S phase with none in G₂ phase (Fig. 2D). For validation, we isolated EB day 6 progenitors and allowed them to expand in vitro for an additional 5 days. Immunostaining with Ki67, a marker for actively cycling cells, showed that 24 hours after isolation, most cells were actively cycling, but this activity decreased over 5 days. Conversely, total cell number increased fourfold over the same 5-day period (Fig. 2E). Furthermore, the expression of the progenitor markers *Isl1* or *Tbx5* was maximal at the time of progenitor isolation but decreased with further differentiation (fig. S8). In contrast, Troponin T expression continued to increase with differentiation (fig. S8). Thus, the progenitor populations have a real but limited in vitro expansion potential. The drop off in expansion is concomitant with differentiation and loss of progenitor marker expression, suggesting that an endogenous clock may limit their proliferative capacity.

To examine progenitor myogenic potential, we cultured embryonic- and ESC-derived progenitors on either fibronectin-coated slides or micropatterns of 20- μ m-wide lines of fibronectin alternating with 20- μ m-wide lines of Pluronic F127 (a surfactant that blocks cell adhesion). After 5 days of in vitro expansion and differentiation, we performed immunofluorescence staining for sarcomeric α -actinin and smooth muscle myosin heavy chain (smMHC), labeling cardiomyocytes and smooth muscle, respectively. Plating embryonic- and ESC-derived R+G+ cells on micropatterned surfaces resulted in anisotropic tissue consisting of longitudinally aligned myocardial fibers (Fig. 3, A and B). In contrast, plating the progenitor populations on unpatterned slides resulted in isotropic unaligned tissue (fig. S9). Cell counting showed that embryonic- and ESC-derived R+G+ progenitors primarily gave rise to cardiomyocytes independent of surface culture conditions. In contrast, the R+G- and R-G+ populations gave rise to a more heterogeneous population of both smooth muscle and cardiomyocytes (Fig. 3, C and D). It remains unclear whether these cells represent homogenous populations of multipotent progenitors or heterogeneous populations of unipotent progenitors. Culturing R+G- (but not other) progenitors on micropatterned surfaces resulted in a statistically significant increase in the proportion of cardiac myocytes, suggesting that this population's myogenic potential may be modulated by microenvironmental geometric cues. Single-cell patch clamp experiments demonstrated that R+G+ progenitors differentiated into ventricular cardiac myocytes with typical four-phase action potential (AP), whereas R+G- and R-G+ progenitors differentiated into more heterogeneous cell types (Fig. 4, A and B; fig. S10; and table S4). Further, R+G+ cardiomyocytes showed sodium-

channel dependency, consistent with ventricular APs (fig. S11).

Next, we used the R+G+ progenitors to engineer two-dimensional cardiac tissue into a muscular thin film (MTF), as described in the supporting online material (SOM) and (15). The MTF beat spontaneously at a rate of ~20 contractions per minute and could be paced by field stimulation at 0.5 and 1.0 Hz. To measure contractility, the MTF was fixed as a cantilever on one end, and the contracting cardiomyocytes bent the MTF toward the cell side during systole (Fig. 4C and movie S1). During diastole, the elastic polydimethylsiloxane film provided the antagonistic force that returned the MTF back to the relaxed position. The change in radius of curvature is inversely proportional to cardiomyocyte stress generation and was measured at ~5 kPa for the progenitor-derived cardiac tissue at peak systole (fig. S12), similar to MTFs engineered from neonatal rat ventricular cardiomyocytes (15).

This development of an in vivo multicolor reporter system in embryos and ESC lines now allows for the purification of distinct subsets of the earliest heart field progenitors. Whereas *Isl1* primarily marks the SHF (4, 16–18), there have been no distinct markers for the FHF lineages that contribute to the LV. Here we document distinct transcriptional signatures for the FHF and SHF lineages, including the expression of unique subsets of miRNAs, which suggest that these lineages have distinct identities. The identification of independent FHF markers should allow a rigorous analysis of their role in heart development and disease.

A critical step in cardiogenesis is the formation and expansion of the ventricular myocyte lineage. The discovery and purification from embryos and corresponding ESC lines of committed ventricular progenitors (CVPs) uncovers a mechanistic pathway for organogenesis through limited expansion and assembly of CVPs into fully functional ventricular muscle tissue. Thus, directed differentiation from multipotent islet progenitors to a specific differentiated progeny occurs via the formation of transient committed intermediate progenitors that are destined to become specific cell types. This finding suggests a general paradigm for the conversion of multipotent islet progenitors to other differentiated cell types, such as endothelial or conduction system cells (fig. S13). Furthermore, recent work has now identified multiple *Isl1* intermediate progenitor populations in human embryonic hearts and human ESCs (19), suggesting that it may be possible to isolate self-expanding human ventricular progenitors.

A central challenge for cell-based therapy has been the identification of an optimal cell type to drive robust cardiac myogenesis. The ideal heart progenitor cell would be derived from a renewable cell source in sufficient quantities to drive clinically relevant levels of cardiac myogenesis. In addition, it would be critical to direct the dif-

ferentiation of progenitor cells into functional ventricular myocytes, instead of related lineages such as smooth muscle cells. The ability to generate functional ventricular MTF from these progenitor cells displaying limited expansion potential should allow the direct chemical screening of previously unknown molecular entities for therapeutic endpoints that can only be measured on intact muscle tissue, including force development and conduction velocity. With recent advances in the generation of induced pluripotent stem cells (20–22), it should now be possible to isolate patient- and disease-specific cardiac progenitors. The combination of tissue engineering technology with stem cell biology, therefore, represents an approach for the development of human models of human disease and a platform for drug discovery and design.

References and Notes

1. M. Buckingham, S. Meilhac, S. Zaffran, *Nat. Rev. Genet.* **6**, 826 (2005).
2. S. Martin-Puig, Z. Wang, K. R. Chien, *Cell Stem Cell* **2**, 320 (2008).
3. E. Dodou, S. M. Xu, B. L. Black, *Mech. Dev.* **120**, 1021 (2003).
4. Y. Qyang *et al.*, *Cell Stem Cell* **1**, 165 (2007).
5. Materials and methods are available as supporting material on Science Online.
6. C. L. Lien *et al.*, *Development* **126**, 75 (1999).
7. S. M. Wu *et al.*, *Cell* **127**, 1137 (2006).
8. E. Dodou, M. P. Verzi, J. P. Anderson, S. M. Xu, B. L. Black, *Development* **131**, 3931 (2004).
9. M. P. Verzi, D. J. McCulley, S. De Val, E. Dodou, B. L. Black, *Dev. Biol.* **287**, 134 (2005).
10. M. Reich *et al.*, *Nat. Genet.* **38**, 500 (2006).
11. B. G. Bruneau *et al.*, *Cell* **106**, 709 (2001).
12. A. D. Mori *et al.*, *Dev. Biol.* **297**, 566 (2006).
13. A. Barrallo-Gimeno, M. A. Nieto, *Development* **132**, 3151 (2005).
14. M. J. Blanco *et al.*, *Development* **134**, 4073 (2007).
15. A. W. Feinberg *et al.*, *Science* **317**, 1366 (2007).
16. K. L. Laugwitz *et al.*, *Nature* **433**, 647 (2005).
17. A. Moretti *et al.*, *Cell* **127**, 1151 (2006).
18. C. L. Cai *et al.*, *Dev. Cell* **5**, 877 (2003).
19. L. Bu *et al.*, *Nature* **460**, 113 (2009).
20. K. Takahashi *et al.*, *Cell* **131**, 861 (2007).
21. J. Yu *et al.*, *Science* **318**, 1917 (2007); published online 19 November 2007 (10.1126/science.1151526).
22. J. Hanna *et al.*, *Cell* **133**, 250 (2008).
23. We thank L. Prickett and K. Folz-Donahue for expert help with flow cytometry. Financial support was provided by the de Gunzburg Family Foundation (to I.J.D.), the NIH fellowship support (T32 HL002807 to I.J.D. and M.C.), the Netherlands Organization for Scientific Research (Rubicon 825-07-011 to P.v.d.M.), and the Leducq Foundation (to K.R.C.). The authors have filed patent applications pertaining to the isolation and expansion of islet cells and the development and use of muscular thin film from CVPs as described herein. Microarray data has been uploaded to the National Center for Biotechnology Information–Gene Expression Omnibus database with accession number GSE17513.

Supporting Online Material

www.sciencemag.org/cgi/content/full/326/5951/426/DC1
Materials and Methods
Figs. S1 to S13
Tables S1 to S4
References
Movie S1

5 June 2009; accepted 21 August 2009
10.1126/science.1177350